Application of an Immersed Boundary Treatment in Simulation of Natural Convection Problems with Complex Geometry via the Lattice Boltzmann Method

R. Khazaeli, S. Mortazavi[†], M. Ashrafizaadeh

Department of Mechanical Engineering, Isfahan University of Technology, Isfahan, 84156-83111, Iran

[†]*Corresponding Author Email:* saeedm@cc.iut.ac.ir

ABSTRACT

In this study, a version of thermal immersed boundary-Lattice Boltzmann method (TIB-LBM) is used to simulate thermal flow problems within complex geometries. The present approach is a combination of the immersed boundary method (IBM) and the thermal lattice Boltzmann method (TLBM) under the double population approach. The method combines two different grid systems, an Eulerian grid for the flow domain and a Lagrangian grid for the boundary points immersed in the flow. In the present method, an unknown velocity correction is considered on the boundary points to impose the no-slip boundary condition. As a similar approach, an unknown internal energy correction on the boundary points is applied to satisfy the constant temperature boundary condition. The advantages of this approach are its second-order accuracy and straightforward calculation of the Nusselt number. The natural convection in an annulus with various outer cylinder shapes for different Rayleigh numbers have been simulated to demonstrate the capability and the accuracy of present approach. In terms of accuracy, the predicted results show an excellent agreement with those predicted by other experimental and numerical approaches.

Keywords: Immersed boundary approach; Thermal lattice Boltzmann method; Fluid flow; Heat transfer; Complex geometry.

1. INTRODUCTION

The recent developments of computer sciences have led to an increase in the utilization of numerical simulations to analyze convoluted phenomena without costly utilization and difficult experimental measurements. In this regard, many different methods have been employed to simulate flows within complex geometries. The conventional approaches use the body-fitted grids for simulation of problems involving complex geometries but the grid generation for such complex geometries is difficult and its quality affects the numerical accuracy severely. The utilization of unstructured grids for complex geometries, resolves partly the grid generation problem of complex geometries but these approaches have in general, a slower convergence rate. On the other hand, to simulate the phenomena involving moving boundaries re-gridding is necessary, which in turn increases the computational cost and difficulty of the method.

So far, many studies have been conducted to alleviate the difficulties associated with the use of body-fitted grid generation methods. The immersed boundary method (IBM) has emerged as a different method from conventional body-fitted approaches especially in the simulation of phenomena involving complex geometries with stationary or moving boundaries. This offers a good flexibility in handling complex geometries but also preserves most of the advantages of structured grid properties. In this method, a simple Cartesian grid is used instead of the body-fitted grid, which eliminates the body-fitted grid generation difficulties and therefore decreases the simulation costs.

The IBM was originally proposed by Peskin (1972) for simulation of the fluid flexible structure interaction problems (the blood flow in the heart). In this approach, a fixed Eulerian grid and a set of Lagrangian points has been used to represent the fluid field and the physical boundaries, respectively. Also, many other methods based on the Peskin work have been emerged to modify or refine the IBM. A review of these methods can be found in Mittal and Iaccarino (2005); Margnat and Morinière (2009). However, much attention has recently been made towards combining IBM with other numerical approaches, e.g. the finite element method and the lattice Boltzmann method (LBM). The lattice Boltzmann method (LBM) (Qian et al. 1992; Chen and Doolen 1998) has been presented in recent years as a viable alternative to conventional computational fluid dynamics (CFD). Unlike standard numerical

methods, which are based on the discretization of macroscopic governing equations, the LBM is based on mesoscopic kinetic equations, which represents characteristics of flow due to the evolution of a single particle velocity distribution. The LBM is easy to implement, numerically stable, computationally efficient, highly accurate and straight forward for parallelization.

In the last years, many methods have been proposed to impose hydrodynamic boundary condition for the LBM. The bounce-back approach (Cornubert et al. 1991), half-way bounce-back approach (Ziegle 1993), hydrodynamic method (Noble et al. 1995), non-equilibrium bounce-back method (Zou and He 1997), and the extrapolation scheme (Chen et al. 1996) are among the popular choices.

On the other hand, several thermal lattice Boltzmann methods (TLBM) have been proposed to satisfactorily simulate heat transfer problems. In general, current lattice Boltzmann methods for thermal flows can be classified into three categories: the multispeed model (Namara and Alder 1993; Alexander et al. 1993), the passive scalar model (Bartoloni et al. 1993; Shan 1997) and the double population model. The multispeed models suffer from intense numerical instability, and can be used for a narrow temperature range. In the multispeed approach, only the density distribution function has been used, but the internal energy equation has been obtained by further discrete velocities. In the passive-scalar model, an independent internal energy distribution function has been used to obtain the temperature field. This model has a better numerical stability compared with the multi-speed model but the viscous dissipation and compression work done by the pressure have been neglected. The double population model introduced by He et al. (1998), similar to passive-scalar models, contains an independent internal energy distribution function but has a better numerical stability. Besides, in this model, the viscous dissipation term and the compression work done by pressure have been taken into account. However, due to contribution of a complicated gradient operator term in the thermal lattice Boltzmann equation (TLBE) the implementation of this technique is not easy. Consequently, several simplified models have been proposed in which the effects of pressure work and/or viscous dissipation in the energy equation have been neglected (Peng et al. 2003; Shi, Zhao and Guo 2004; Li et al. 2008). In order to enhance stability of these models some researchers proposed Multi-Relaxation-Time TLBM (Teixeira et al. 2000; Rahmati et al .2014)

Recently, Fu et al. (2012) developed a finite difference approach based on a linearized-Boltzmann-type-equation for thermal incompressible flows with external body force effect. To ensure incompressibility, the pressure field is obtained by a pressure-correction approach in this method.

So far, several approaches have been proposed to satisfactorily impose thermal boundary conditions for the TLBE (Tang et al. 2005; D'Orazio et al. 2004; Liu et al.

2010). However, due to some limitations in the standard LBM (e.g. the requirement of using uniform orthogonal lattices and a constant time step), it is not so easy to implement boundary conditions for complex geometries. To alleviate such difficulties, several attempts have been conducted (Kao and Yang 2008). One of these attempts proposes a combination of the LBM and the IBM which results in the development of the hybrid immersed boundary lattice Boltzmann method (IBLBM). Originally, Feng and Michaelides (Feng and Michaelides 2004; Feng and Michaelides 2005) successfully used the IBLBM to simulate particulate flows. Niu et al. (2006) proposed the momentum-exchange-based immersed boundary lattice Boltzmann method by using a multi-relaxation collision model in which the forcing term was calculated through the implementation of the momentum exchange role on boundary nodes. Peng et al. (2006) developed the multi-block IBLBM to simulate flows around a circular cylinder and an airfoil. Wu and Shu (2009) proposed an implicit velocity correction-based IBLBM which implicitly satisfies the no-slip boundary condition by considering an unknown velocity correction vector at each boundary point. Kang and Hassan (2010) compared various IBLBMs with single and multiple step forcing methodologies and proposed a second order sharp interface scheme to handle the complex geometries via the LBM. Recently, Fu et al. (2013a,b) developed a finite difference LBM with an immersed boundary method to simulate blood flow in constricted pipes.

To the best of the author's knowledge, there are only a few proposed IB-LBM models in the open literature for handling both fluid flow and heat transfer phenomena. The work of Jeong et al. (2010) may be considered as the first research work in this respect. They used feedback forcing scheme to impose the curve boundary condition for both energy and momentum fields and simulated thermal flows around bluff bodies. However, this approach suffers from defects such as instability and arbitrariness in selecting the related parameters (He et al. 1998; Kang and Hassan 2011). Furthermore, the implementation of this technique has been complicated using the complex double-population model (He et al. 1998). Afterwards, Kang and Hassan (2011) utilize the coupling between the IBM and the TLBM to simulate thermal flows. They adopted the sharp interface scheme based on second-order bilinear and linear interpolations and used two thermal LB models: a double-population model with a simplified thermal lattice Boltzmann equation and a hybrid model with an advection-diffusion equation for temperature. Khazaeli et al. (2013) proposed a curved boundary treatment based on the combination of a ghost fluid approach and the bounce-back method to simulate thermal problems with complex geometries. Seta (2013) applied the implicit-correction approach to the immersed-boundary thermal lattice Boltzmann method to simulate natural convection between two concentric horizontal cylinders. He also founded that IB-TLBM requires a small relaxation time to avoid distortion of temperature around the solid boundary.

In the present study, however, we have adopted the scheme presented by Wu and Shu (2009) and Kang and Hassan (2011) to enhance the ability of thermal lattice Boltzmann method in dealing with curved

boundary condition. In this paper, we use the IB-LBM proposed by Wu and Shu (2009) to satisfy the no-slip boundary condition at curved boundary and then the method is extended to a simplified internal energy LBE with an energy source term (Wang, Wang and Li 2007; Kang and Hassan 2011). Similar to the implementation of velocity correction in IB-LBM (Wu and Shu 2009), the thermal boundary condition can be satisfied implicitly using an internal energy correction on the boundary surface. Our strategy is based on the utilization of the forcing concept, and benefits from advantages such as second-order accuracy and easy calculation of the Nusselt number. The validity of the method is finally verified through simulating two natural convection heat transfer problems. The rest of the paper is organized as follows. Section 2.1 reviews the implicit velocity correction-based IBM for the isothermal LBM proposed by Wu and Shu (2009). In Section 2.2, this IB method is extended to a simplified thermal LBE with an energy source term (Wang et al. 2007; Kang and Hassan 2011). Detailed numerical simulations are performed within Section 3 and the results obtained by the present method are compared with experimental and computational results. Finally, Section 4 summarizes the content of the paper and presents the conclusions.

2. NUMERICAL METHODS

2. 1. Implicit Velocity Correction-Based Immersed Boundary for the Isothermal lattice Boltzmann Equation

Here, the approach proposed by Wu and Shu (2009) is used to impose the curved boundary conditions. In this method, the single-relaxation-time LBE proposed by Guo et al. (2002) is adopted, which can be expressed as:

$$f_i(\mathbf{x} + \mathbf{e}_i \delta t, t + \delta t) - f_i(\mathbf{x}, t) =$$
$$-\frac{1}{\tau}(f_i(\mathbf{x},t) - f_i^{eq}(\mathbf{x},t)) + F_i \delta t \tag{1}$$

$$F_i = (1 - \frac{1}{2\tau})w_i(\frac{\mathbf{e}_i - \mathbf{u}}{c_s^2} + \frac{\mathbf{e}_i \cdot \mathbf{u}}{c_s^4} \cdot \mathbf{e}_i) \cdot \mathbf{f} \tag{2}$$

$$\rho\mathbf{u} = \sum_i \mathbf{e}_i f_i + \frac{1}{2}\mathbf{f}\delta t \tag{3}$$

where, f_i is the density distribution function, f_i^{eq} is the equilibrium density distribution function, τ is the dimensionless relaxation time, F_i is the external force in the direction of the lattice velocity, $\mathbf{f}$ is the force density and w_i is weighting coefficient which depends on the discrete velocity set. Here we have used the popular D2Q9 lattice velocity model where we have:

$$e_\alpha = \begin{cases} 0 \\ \left(\cos\left[(i-1)\pi/2\right], \sin\left[(i-1)\pi/2\right]\right) \\ \sqrt{2}\left(\cos\left[(i-5)\pi/2+\pi/4\right], \sin\left[(i-5)\pi/2+\pi/4\right]\right) \end{cases}$$

$$i = 0$$
$$i = 1,2,3,4$$
$$i = 5,6,7,8 \tag{4}$$

For this model, the density equilibrium distribution function, f_i^{eq}, in Eq. (1) is given by:

$$f_i^{eq}(\mathbf{x},t) = \rho w_i \begin{bmatrix} 1 + \frac{3}{c^2}(\mathbf{e}_i \cdot \mathbf{u}) + \frac{4.5}{c^4}(\mathbf{e}_i \cdot \mathbf{u})^2 \\ -\frac{1.5}{c^2}u^2 \end{bmatrix} \tag{5}$$

Here, $w_0 = 4/9$, $w_i = 1/9$, $(i = 1,2,3,4)$ and $w_i = 1/36$, $(i = 5,6,7,8)$. $c = \Delta x/\Delta t$ is the lattice speed and Δx and Δt are the lattice size and the time step, respectively. The kinematic viscosity, υ, is determined by:

$$\upsilon = \left(\tau - \frac{1}{2}\right)c_s^2 \Delta t \tag{6}$$

where c_s is the speed of sound and is related to the lattice speed, c, by $c_s = c/\sqrt{3}$. As can be seen from Eq. (3), the fluid velocity is composed of two parts. The first part is due to the density distribution function and the second part is related to the force density, $\mathbf{f}$. Then we can rewrite Eq. (3) as follow:

$$\mathbf{u} = \mathbf{u}^* + \delta\mathbf{u} \tag{7}$$

$$\mathbf{u}^* = \frac{1}{\rho}\sum_i \mathbf{e}_i f_i \tag{8}$$

$$\delta\mathbf{u} = \frac{1}{2\rho}\mathbf{f}\delta t \tag{9}$$

Here, $\mathbf{u}^*$ is the intermediate velocity and $\delta\mathbf{u}$ is the velocity correction. With a closer look at imposing boundary condition in the direct forcing methods, it is clearly seen that there is no guarantee to satisfy the no-slip boundary condition by the interpolated velocities at the boundary points (Wu and Shu 2009).
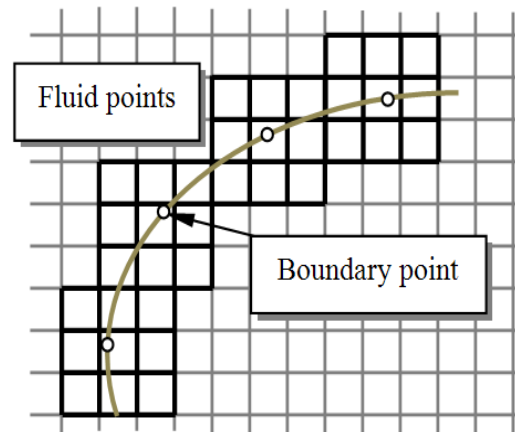
Fig. 1. Schematic diagram of configuration of boundary points and their surrounding fluid points.

To resolve this problem, an unknown force term at the boundary point can be considered (Wu and Shu 2009), such that the interpolated velocity at the boundary point satisfies the no-slip boundary condition. According to the idea of IBM, the boundary surface of body is indicated by a set of Lagrangian points $X_B(s_l,t)$, $l = 1,2,$

.., m. So, by setting an unknown velocity correction vector $\delta\mathbf{u}_B$ at every boundary point (with position of $\mathbf{X}_B$), we can define the velocity correction component at every Eulerian point using the interpolation by the smooth delta function as shown in Fig. 1. Hence, the velocity correction component at Eulerian points can be defined as:

$$\delta\mathbf{u}(\mathbf{x},t) = \int_\Gamma \delta\mathbf{u}_B(X_B,t)\delta(\mathbf{x}-X_B(s,t))ds \tag{10}$$

where, $\delta(\mathbf{x}-X_B(s,t))$ is approximated as:

$$\delta(\mathbf{x}-X_B(s,t)) = D_{ij}(x_{ij}-X_B^l) =$$
$$\delta(x_{ij}-X_B^l)\delta(y_{ij}-Y_B^l) \tag{11}$$

Here, in order to increase accuracy of method we used a discrete delta function proposed by Yang et al. (2009) instead of Peskin's function (Peskin 1972):

$$\delta(r) = \begin{cases} \begin{aligned} &\frac{17}{48} + \frac{\sqrt{3}\pi}{108} + \frac{|r|}{4} - \frac{r^2}{4} + \frac{1-2|r|}{16}\sqrt{-12r^2+12|r|+1} \\ &- \frac{\sqrt{3}}{12}\arcsin\left(\frac{\sqrt{3}}{2}(2|r|-1)\right), \qquad |r|\leq 2, \\[4pt] &\frac{55}{48} - \frac{\sqrt{3}\pi}{108} - \frac{13|r|}{12} + \frac{r^2}{4} + \frac{2|r|-3}{48}\sqrt{-12r^2+36|r|-23} \\ &+ \frac{\sqrt{3}}{36}\arcsin\left(\frac{\sqrt{3}}{2}(2|r|-3)\right), \qquad 1\leq|r|\leq 2, \\[4pt] &0, \qquad\qquad\qquad\qquad\qquad\qquad |r| > 2, \end{aligned} \end{cases} \tag{12}$$

in which h is the boundary surrounding the Eulerian mesh spacing. Using Eqs. (10) and (11), the velocity correction values at the boundary points are determined by:

$$\delta\mathbf{u}(x_{ij},t) = \sum_{l=1}^{m}\delta\mathbf{u}_B^l(X_B^l,t)D_{ij}(x_{ij}-X_B^l)\Delta s_l \tag{13}$$

where, Δs_l is the arc length of the boundary element. According to Eq. (7), the velocity of fluid at the Lagrangian points can be evaluated as:

$$\mathbf{u}(x_{ij},t) = \mathbf{u}^*(x_{ij},t) + \delta\mathbf{u}(x_{ij},t) \tag{14}$$

where, $\mathbf{u}^*$ is the intermediate velocity of fluid, which is obtained from Eq. (8). To impose the no-slip boundary condition, the fluid velocities at the Lagrangian points obtained through the interpolation, must be equal to the desired boundary velocities $U_B^l(X_B^l,t)$ at the same Lagrangian points.

$$U_B^l(X_B^l,t) = \sum_{i,j}\mathbf{u}(x_{ij},t)D_{ij}(x_{ij}-X_B^l)\Delta x\Delta y \tag{15}$$

Substituting Eq. (14) and Eq. (13) into Eq. (15) gives:

$$U_B^l(X_B^l,t) = \sum_{i,j}\mathbf{u}^*(x_{ij},t)D_{ij}(x_{ij}-X_B^l)\Delta x\Delta y +$$
$$\sum_{i,j}\sum_{l}\delta\mathbf{u}_B^l(X_B^l,t)D_{ij}(x_{ij}-X_B^l)\Delta s_l D_{ij}(x_{ij}-X_B^l)\Delta x\Delta y \tag{16}$$

The matrix form of Eq. (16) can be expressed as:

$$AX = B \tag{17}$$

where, in this relation

$$X = \left\{\delta\mathbf{u}_B^1, \delta\mathbf{u}_B^2, ..., \delta\mathbf{u}_B^m\right\} \tag{18}$$

$$A = \begin{pmatrix} \delta_{11} & \delta_{12} & \cdots & \delta_{1n} \\ \delta_{21} & \delta_{22} & \cdots & \delta_{2n} \\ \vdots & \vdots & \ddots & \vdots \\ \delta_{m1} & \delta_{m2} & \cdots & \delta_{mn} \end{pmatrix}\begin{pmatrix} \delta_{11}^B & \delta_{12}^B & \cdots & \delta_{1n}^B \\ \delta_{21}^B & \delta_{22}^B & \cdots & \delta_{2n}^B \\ \vdots & \vdots & \ddots & \vdots \\ \delta_{m1}^B & \delta_{m2}^B & \cdots & \delta_{mn}^B \end{pmatrix} \tag{19}$$

$$B = \begin{pmatrix} U_B^1 \\ U_B^2 \\ \vdots \\ U_B^m \end{pmatrix} - \begin{pmatrix} \delta_{11} & \delta_{12} & \cdots & \delta_{1n} \\ \delta_{21} & \delta_{22} & \cdots & \delta_{2n} \\ \vdots & \vdots & \ddots & \vdots \\ \delta_{m1} & \delta_{m2} & \cdots & \delta_{mn} \end{pmatrix}\begin{pmatrix} u_1^* \\ u_2^* \\ \vdots \\ u_n^* \end{pmatrix} \tag{20}$$

Here, m is the number of Lagrangian points and n is the number of Eulerian points, which has been used in the interpolation by the smooth delta function. By solving this system of equations using a direct approach or iterative technique, the unknown velocity correction components at the boundary points, $\delta\mathbf{u}_B^l$, can be determined. Then, the velocity correction values at the Eulerian points and the fluid corrected velocity values can be defined using Eqs. (13) and (14), respectively. Also, the force at the boundary points can be determined easily as follows:

$$\mathbf{f} = 2\rho\delta\mathbf{u}/\delta t \tag{21}$$

The density and the pressure in LBM, is evaluated as:

$$\rho = \sum f_\alpha, \quad P = C_s^2\rho. \tag{22}$$

2.2. Implicit internal energy correction-based immersed boundary treatment for the thermal lattice Boltzmann equation

The Simplified thermal lattice Boltzmann model proposed by Peng et al. (2003) with an energy source term is used as the thermal model in this study.

$$g_i(\mathbf{x}+\mathbf{e}_i\delta t, t+\delta t) - g_i(\mathbf{x},t) =$$
$$-\frac{1}{\tau_g}(g_i(\mathbf{x},t) - g_i^{eq}(\mathbf{x},t)) + Q_i\Delta t \tag{23}$$

Here, τ_g denotes the lattice relaxation time for the temperature field, g_i is the internal energy density distribution function and g_i^{eq} is the equilibrium internal energy density distribution function, which can be written as follows:

$$g_i^{eq}(\mathbf{x},t) = \begin{cases} w_i\rho e\left(-\frac{1.5}{c^2}u^2\right), & i=0 \\[8pt] w_i\rho e\left(\begin{aligned}&1.5 + \frac{3}{c^2}(\mathbf{e}_i\cdot\mathbf{u}) + \\ &\frac{4.5}{c^4}(\mathbf{e}_i\cdot\mathbf{u})^2 - \frac{1.5}{c^2}u^2\end{aligned}\right), & i=1,2,3,4 \\[12pt] w_i\rho e\left(\begin{aligned}&3 + \frac{6}{c^2}(\mathbf{e}_i\cdot\mathbf{u}) + \\ &\frac{4.5}{c^4}(\mathbf{e}_i\cdot\mathbf{u})^2 - \frac{1.5}{c^2}u^2\end{aligned}\right), & i=5,6,7,8 \end{cases} \tag{24}$$

Here, $c = \sqrt{3RT_0}$ is the lattice speed, with R and T_0 being the gas constant and a reference temperature, respectively, and e is the internal energy defined as $e = DRT/2$, where, D represents the dimension of the problem and T is the reference temperature. In this paper, *2D* problems are only considered. The discrete energy source function Q_i is defined as:

$$Q_i = w_i\left(1 - \frac{1}{2\tau_g}\right)Q \tag{25}$$

where, Q is the energy source density term. The macroscopic internal energy is determined by:

$$\rho e = \sum_i g_i + \frac{\Delta t}{2}Q \tag{26}$$

The thermal diffusivity α is then related to the relaxation time by:

$$\alpha = \left(\tau_g - \frac{1}{2}\right)c_s^2 \Delta t \tag{27}$$

As seen, in this model, the internal energy comprises two parts. The first part is due to the the internal energy density distribution function and the second part is related to the energy source term.

$$e = e^* + \delta e \tag{28}$$

$$e^* = \frac{1}{\rho}\sum_i \mathbf{e}_i g_i \tag{29}$$

Here, δe is the internal energy correction and e^* is the intermediate internal energy. Now, similar to the velocity correction implementation, by setting an unknown internal energy correction at every Lagrangian point, the internal energy correction values at the Eulerian points can be obtained using the interpolation by the smooth delta function.

$$\delta e(\mathbf{x}_{ij}, t) = \sum_{l=1}^{m} \delta e_B^l(X_B^l, t) D_{ij}(\mathbf{x}_{ij} - X_B^l)\Delta s_l \tag{30}$$

So the corrected internal energy values at the Eulerian points, can be determined as:

$$e(\mathbf{x}_{ij}, t) = e^*(\mathbf{x}_{ij}, t) + \delta e(\mathbf{x}_{ij}, t) \tag{31}$$

To satisfy the constant temperature boundary condition, the internal energy values at the Lagrangian points obtained by interpolation, must be equal to the desired boundary internal energy $E_B^l(X_B^l, t)$ values at the same Lagrangian points. So similar to the previous approach, a similar system of equations can be obtained as follow:

$$CY = D \tag{32}$$

$$Y = \left\{\delta e_B^1, \delta e_B^2, ..., \delta e_B^m\right\} \tag{33}$$

$$C = \begin{pmatrix} \delta_{11} & \delta_{12} & \cdots & \delta_{1n} \\ \delta_{21} & \delta_{22} & \cdots & \delta_{2n} \\ \vdots & \vdots & \ddots & \vdots \\ \delta_{m1} & \delta_{m2} & \cdots & \delta_{mn} \end{pmatrix} \begin{pmatrix} \delta_{11}^B & \delta_{12}^B & \cdots & \delta_{1n}^B \\ \delta_{21}^B & \delta_{22}^B & \cdots & \delta_{2n}^B \\ \vdots & \vdots & \ddots & \vdots \\ \delta_{m1}^B & \delta_{m2}^B & \cdots & \delta_{mn}^B \end{pmatrix} \tag{34}$$

$$D = \begin{pmatrix} E_B^1 \\ E_B^2 \\ \vdots \\ E_B^m \end{pmatrix} - \begin{pmatrix} \delta_{11} & \delta_{12} & \cdots & \delta_{1n} \\ \delta_{21} & \delta_{22} & \cdots & \delta_{2n} \\ \vdots & \vdots & \ddots & \vdots \\ \delta_{m1} & \delta_{m2} & \cdots & \delta_{mn} \end{pmatrix} \begin{pmatrix} e_1^* \\ e_2^* \\ \vdots \\ e_n^* \end{pmatrix} \tag{35}$$

By solving this system of equations, the unknown correction of internal energy values at the Lagrangian points can be determined and then the correction of internal energy values at the Eulerian points are obtained using Eq. (30). The value of internal energy source density term in Eqs. (25) and (26) can be evaluated as:

$$Q = 2\rho\, \delta e / \delta t \tag{36}$$

Note here that, at all boundaries, the bounce-back scheme is used for both of the hydrodynamic and thermal boundary conditions (Kang and Hassan 2011). For all the simulations in the present study the following convergence criteria are used.

$$\max\left[\left|\sqrt{\left(u^{n+1}\right)^2 + \left(v^{n+1}\right)^2} - \sqrt{\left(u^n\right)^2 + \left(v^n\right)^2}\right|\right] \leq 10^{-9}$$

$$\max\left[\left(\sqrt{\left(T^{n+1} - T^n\right)}\right)\right] \leq 10^{-9} \tag{37}$$

Here, n and n + 1 demonstate the old and the new time levels, respectively. Also, the following criterion based on the relative L2-norm error, E, is adopted to estimate the overall accuracy of the method.

$$E = \left|Nu_{avg} - Nu_{avg}^{exact}\right| \tag{38}$$

where, the superscript $\{exact\}$ refers to the exact solution of problem under consideration.

3. RESULTS AND dISCUSSIONS

3.1. Natural Convection in a Square Cavity

In order to demonstrate the validity of the present thermal LBM code, the natural convection problem in a square cavity is investigated. The configuration of the natural convection in a square cavity is shown in Fig. 2, which consists of a 2-D square cavity of length L with a hot wall on the left side (with the temperature T_h) and a cold wall on the right side (with the temperature T_c), while the other side walls are adiabatic. The temperature difference between the left and right walls causes a temperature gradient in the flow domain which, in turn, sets the fluid in motion. Here, the fluid properties are assumed constant, except for the density in the buoyancy term, which follows the Boussinesq approximation. However, the mean density value is constant. The external force term $\mathbf{F}$ in Eq. (3), corresponding to buoyancy force in this special case, is given by $\mathbf{F} = -\rho\beta(T - T_0)\mathbf{g}$, where $T_0 = (T_h + T_c)/2$ is the average temperature, β represents the thermal expansion coefficient at T_0, and $\mathbf{g}$ is the gravitational acceleration acting in the negative vertical direction.
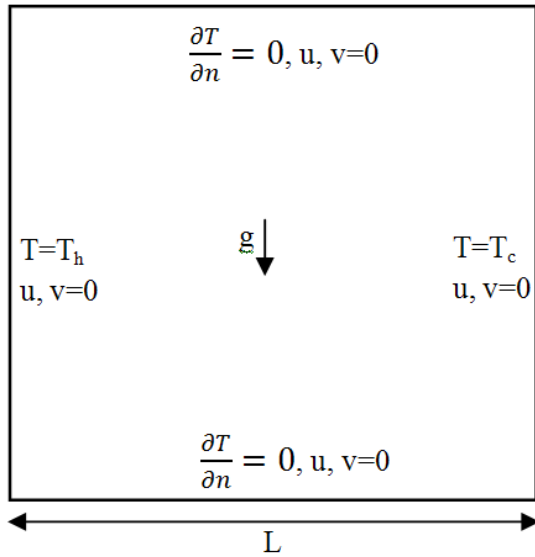
Fig. 2. Schematic diagram of configuration and boundary conditions for natural convection phenomenon in a cavity

The major control parameters for this problem are the Rayleigh number, *Ra*, and the Prandtl number, *Pr* , defined as:

$$Ra = \frac{g\beta\Delta T L^3}{\upsilon\alpha}, \quad Pr = \frac{\upsilon}{\alpha} \tag{39}$$

Note here that, air was considered to be the working fluid and the Prandtl number was set to 0.71. In this study, the characteristic velocity is taken as

$V_c = \sqrt{\beta g \Delta T L}$. Therefore, the viscosity, thermal diffusivity and the relaxation times τ_f and τ_g , can be written as:

$$\upsilon = \sqrt{\frac{Pr}{Ra}} V_c L; \quad \tau_f = 3\sqrt{\frac{Pr}{Ra}} V_c L + \frac{1}{2} \tag{40}$$

$$\alpha = \frac{V_c L}{\sqrt{RaPr}}; \quad \tau_g = \frac{3V_c L}{2\sqrt{RaPr}} + \frac{1}{2} \tag{41}$$

We set $V_c \leq 0.1\, c$ to ensure that the compressibility error remains small. Therefore, we have chosen $V_c = 0.01\, c$ for $Ra = 10^3$ and $V_c = 0.02\, c$ for $Ra = 10^4$, whereas $V_c = 0.1\, c$ for $Ra = 10^5$ and $Ra = 10^6$. A 100×100 uniform grid was used for $Ra = 10^3$ and a 150×150 uniform grid was used for $Ra = 10^4$, whereas a 200×200 uniform grid was used for $Ra = 10^5$ and $Ra = 10^6$. A careful grid study is carried out to insure the independency of the numerical results of the employed mesh. The grid-dependence study for the special value of $Ra = 10^4$ is presented via Table 1. The data in the table includes the numerical results

for the maximum horizontal velocity on the vertical mid-plane of the cavity, w_α , and its location $y_{\max}$, the maximum vertical velocity on the horizontal mid-plane of the cavity, $v_{\max}$, and its location $w_0 = 4/9$, and the surface-averaged Nusselt number at the hot wall of the cavity, Nu_{avg} , was calculated through:

$$Nu = \frac{1}{L}\int_0^L Nu\ ds \ \text{with} \ Nu = -\frac{L}{\Delta T}\frac{\partial T}{\partial n} \tag{42}$$

where, Nu is the local Nusselt number, $\Delta T = T_h - T_c$, and n is the normal direction to the hot wall. The grid size has been selected as N×N, where N is the number of grid in each direction. As is clear, with further increasing the number of grids (N) from $N = 150$ to $N = 200$, no noticeable improvement is observed in the calculated results. Accordingly, we can state that for the special value of $Ra = 10^4$, the grid size of 150×150 is fine enough to obtain accurate results. Performing similar

**Table 1 Grid dependence study for natural convection in a square cavity at Ra=10⁴.**

Mesh	100×100	150×150	200×200	Davis (1983)
u_{max}	16.155	16.179	16.178	16.178
y_{max}	0.825	0.823	0.823	0.823
v_{max}	19.557	19.601	19.612	19.617
x_{max}	0.116	0.118	0.118	0.119
Nu_{avg}	2.241	2.245	2.243	2.243

tests to that described for $Ra = 10^4$, a 100×100 uniform grid is used for the flow with $Ra = 10^3$, whereas a mesh size of 200×200 is employed for the cases with $Ra = 10^5$ and 10^6 .

Table 2 aims to compare our simulation results for x_{max}, y_{max}, u_{max}, v_{max} and Nu_{av} with the results of Davis (1983) and Hortmann et al. (1990), which were obtained by a stream function-vorticity formulation and a finite volume multigrid procedure respectively. One may confirm that in terms of accuracy, the achievements of this study exhibit good agreement with those of the other researchers. From the provided data, it can be inferred that the values of u_{max} , v_{max} , and Nu_{avg} all increase with an increase in the Rayleigh number. Note here that, the reference velocity value of α/L has been used to normalize the velocities presented in the Table 2.

Table 2 Comparison of velocities and Nusselt numbers for natural convection phenomenon in the cavity

		Ra = 10^3	Ra = 10^4	Ra = 10^5	Ra = 10^6
u_{max}	Present	3.647	16.169	34.842	64.701
	Davis (1983)	3.649	16.178	34.730	64.630
	Hortmann et al. (1990)	-	16.176	34.738	64.834
y_{max}	Present	0.813	0.823	0.857	0.850
	Davis 1983	0.813	0.823	0.855	0.850
	Hortmann et al. (1990)	-	0.825	0.855	0.850
v_{max}	Present	3.698	19.614	68.561	220.452
	Davis (1983)	3.697	19.617	68.590	219.360
	Hortmann et al. (1990)	-	19.624	68.636	220.473
x_{max}	Present	0.178	0.118	0.067	0.038
	Davis (1983)	0.178	0.119	0.066	0.038
	Hortmann et al. (1990)	-	0.120	0.066	0.039
Nu_{avg}	Present	1.118	2.249	4.537	8.839
	Davis (1983)	1.118	2.243	4.519	8.800
	Hortmann et al. (1990)	-	2.245	4.521	8.825
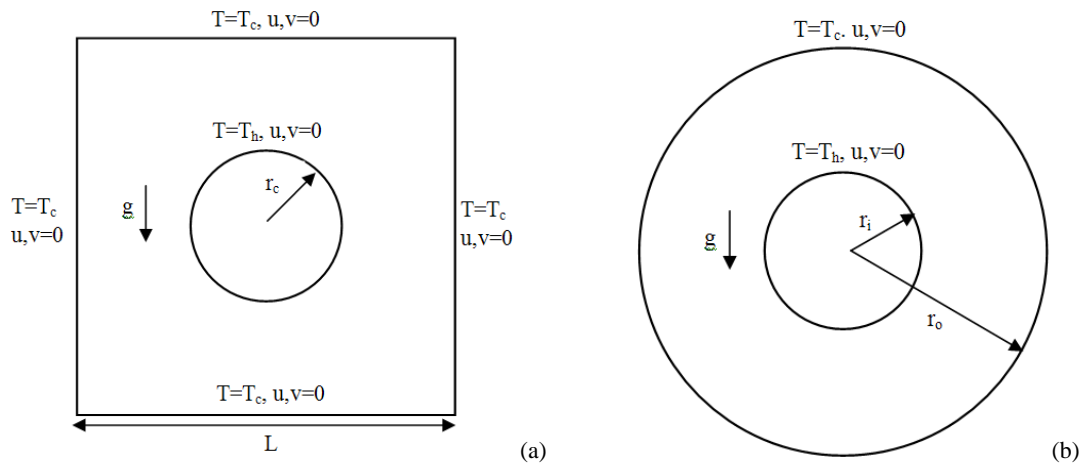
Fig. 3. Schematic diagram of configuration and boundary conditions for natural convection phenomenon in annuluses with different outer shapes (a) square shape (b) circular shape.

3.2. Natural convection in an annulus with various outer cylinder shapes

3.2.1. Natural convection in a concentric annulus with outer square cylinder

In order to validate the present model, we consider the natural convection of fluid in an annulus with outer square cylinder. As can be seen from Fig. 3(a), the geometry involves a two-dimensional square cavity of length L with a concentric circular cylinder of radius Δs_l. The cavity walls are fixed at the cold temperature T_C whereas the cylinder wall is fixed at the hot temperature T_H. Note here that, both cavity and circular cylinder walls are considered to be fixed and without motion. The aspect ratio between the square cylinder and circular cylinder is defined as $\lambda = L/2r_c$ and set to $\lambda = 2.5$. Here, the Prandtl number was set to 0.71

and the Rayleigh number varies in the range of $10^3 \leq Ra \leq 10^6$. We set $V_c = 0.01\,c$ for Rayleigh number 10^3 and $V_c = 0.02\,c$ for Rayleigh number 10^4, whereas $V_c = 0.1\,c$ for Rayleigh number 10^5 and 10^6.

Similar to previous problem, uniform rectangular grids of sizes 100×100 and 150×150 are used for Rayleigh number 10^3 and 10^4, respectively. For Rayleigh numbers 10^5 and 10^6, however, a 200×200 grid is employed. In Fig. 4, the isotherms and streamlines obtained by present method for $Ra = 10^3, 10^4, 10^5$ and 10^6 and $Pr = 0.71$ have been compared with results given by Kim et al. (2008). Note here that, the isotherms contain 11 contour lines whose levels vary

Table 3 Comparison of Nu_{avg} for natural convection in the annulus with square outer shape at different values of Ra

Ra	Nu_{avg}					
	Present	OpenFOAM	Shu and Zhu (2002)	Duy et al. (2008)	Moukalled and Acharya (1996)	Kim et al. (2008)
10^4	3.255	3.225	3.240	3.224	3.331	3.414
10^5	4.933	4.906	4.860	4.901	5.080	5.138
10^6	8.957	8.893	8.900	8.726	9.374	9.39

linearly from the minimum to maximum values. A detailed physical interpretation of the flow and heat transfer phenomena related to this case study is discussed by Kim et al. (2008). As expected, the contours are in very good agreement with those from Kim et al. (2008). The Nusselt number is an important parameter, which is used to estimate the rate of heat transfer in thermal phenomenon. The local Nusselt number on the surface of the circular cylinder is calculated as:

$$Nu = \frac{hL_c}{k} \tag{43}$$

where, L_c is the characteristic length, k is the thermal conductivity coefficient and h is the local convective heat transfer coefficient and can be calculated by:

$$h = \frac{Q}{\Delta T} \tag{44}$$

where, Q is the local convective heat transfer and ΔT is the characteristic temperature difference. So the local Nusselt number can be rewritten as:

$$Nu = \frac{QD}{k\Delta T} \tag{45}$$

We can rewrite Eq. (45) by dividing the denominator and the numerator by ρc_p as:

$$Nu = \frac{Q/\rho c_p \, L_c}{k/\rho c_p \, \Delta T} = \frac{qL_c}{\alpha \Delta T} \tag{46}$$

Here, k is thermal conductivity coefficient, c_p is the specific heat coefficient and q is the local energy-forcing term [34] and can be calculated as:

$$q = Q/\rho c_p = (T^d - T^*)/\Delta t \tag{47}$$

where, T^d is the desired temperature on the cylinder surface and T^* is the intermediate temperature on the Lagrangian points. On the other hand, the local internal energy source term Q_B is defined at the Lagrangian points as:

$$Q_B = 2\rho_B \frac{\delta e_B}{\delta t} = 2\rho_B \frac{c^2}{3T_0} \frac{\delta T_B}{\delta t} \tag{48}$$

where, the relation between the local energy-forcing term q and the local internal energy source term Q_B can be evaluated as:

$$q = \frac{3T_0}{2\rho_B c^2} Q_B \tag{49}$$

Substituting Eq. (49) into Eq. (46) gives:

$$Nu = \frac{3T_0 Q_B L_c}{2\rho_B c^2 \alpha \Delta T} \tag{50}$$

Equation (50) can be rewritten using Eq. (36) as:

$$Nu = \frac{3T_0 \delta e_B^l L_c}{c^2 \alpha \Delta T} \tag{51}$$

By integrating over the surface of the body, the surface averaged Nusselt number Nu_{avg} can be calculated as:

$$Nu_{avg} = \frac{1}{2\pi r_c} \int_\Omega Nu ds = \frac{3T_0 L_c \sum_l \delta e_B^l \Delta s_l}{2\pi r_c c^2 \alpha \Delta T \delta t} \tag{52}$$

For this case study, $\Delta T = (T_h - T_c)$ and the characteristic length L_c is chosen as $S/2$ according to the work of Moukalled and Acharya (1996), where S is the surrounding of inner cylinder So, the surface averaged Nusselt number Nu_{avg} can be calculated as:

$$Nu_{avg} = \frac{3T_0 \sum_l \delta e_B^l \Delta s_l}{2c^2 \alpha (T_h - T_c) \delta t} \tag{53}$$

Table 3 compares our simulation results for Nu_{avg}, at various values of the aspect ratio and for a wide range of the Rayleigh number, with the various numerical approaches (a combination of immersed boundary method and finite volume method, Kim et al. (2008), a boundary-fitted coordinate system using a control volume-based numerical procedure, Moukalled and Acharya (1996), a Cartesian grid technique founded on one-dimensional integrated radial basis function networks, Duy et al.(2008), a differential quadrature (DQ) method, Shu and Zhu (2002)), and also the results obtained by the CFD software package OpenFOAM (OpenSource Field Operation and Manipulation, version 2.1.0, developed by the OpenFOAM Team at SGI Corp).

As seen, the achievements of the present study are in good quantitative agreement with their equivalents in literature. It is also found that both the aspect ratio and the Rayleigh number play critical roles in transport characteristics of the problem. The convergence rates of the relative L_2 error for the averaged Nusselt number Nu_{avg} are plotted logarithmically against the grid spacing Δx in Fig. 5 to test spatial accuracy of the treatment.

$Ra = 10^3$

$Ra = 10^4$

$Ra = 10^5$

(a)   (b) $Ra = 10^6$ (a)   (b)
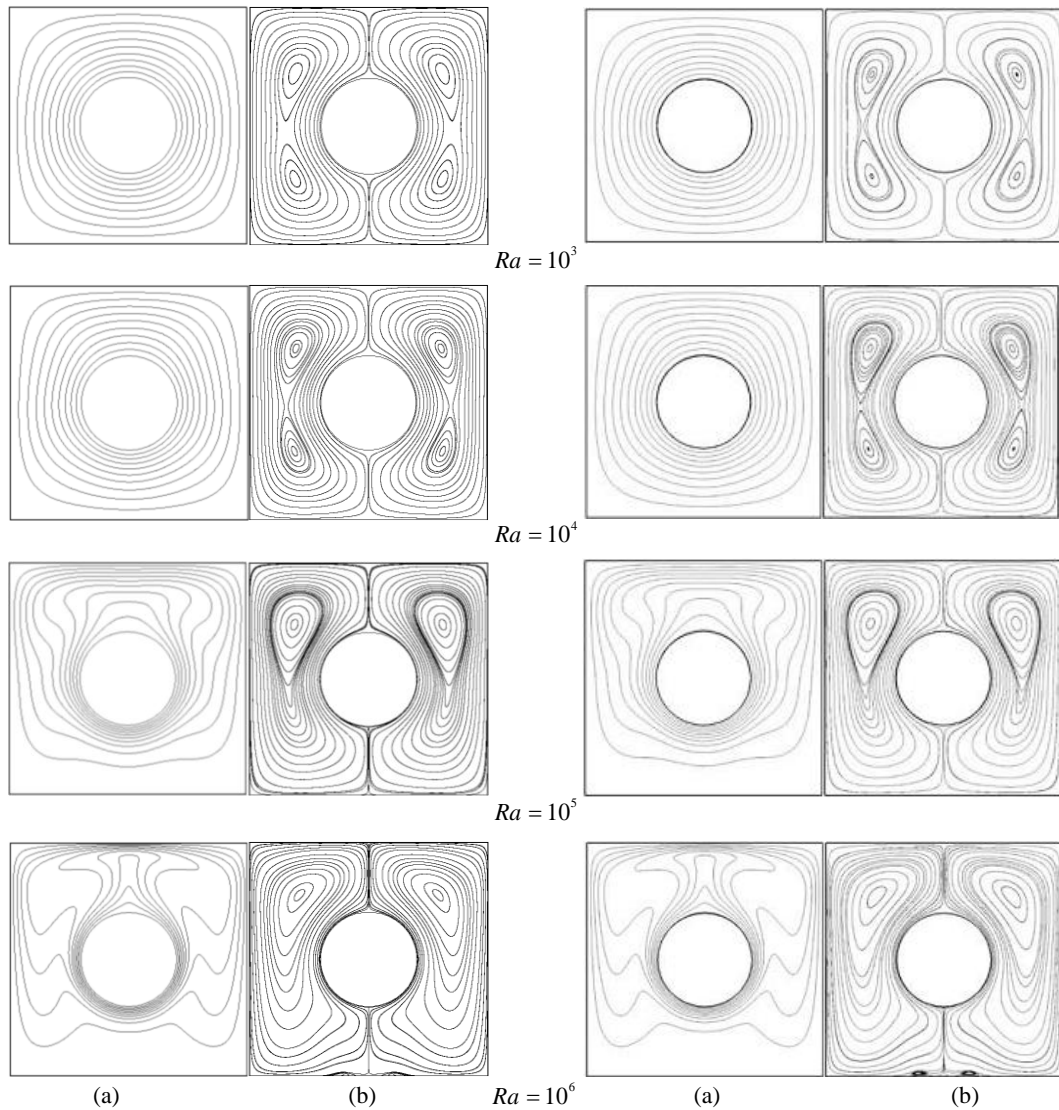
Fig. 4. Comparison of (a) isothermals and (b) streamlines at four different Rayleigh numbers for natural convection phenomenon within an annulus comprised of a circular cylinder in a square enclosure, left: present study; right: Kim et al. (2008).
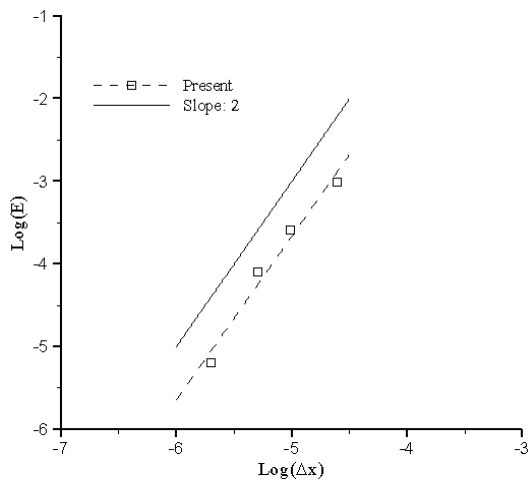

Fig. 5. Relative L_2 norm for the radial velocity and temperature distributions versus the lattice spacing Δx in a log-log scale.

The study is carried out for $Ra = 10^5$ and the number of grids (N) varies from $N = 100$ to $N = 300$. Due to the analytical solution does not exist, the average Nusselt number obtained by $N = 400$ has been considered as an exact solution. As can be inferred from this figure, the slope of the least-squares fit line is 1.98, which confirms the second order accuracy of the overall numerical approach.

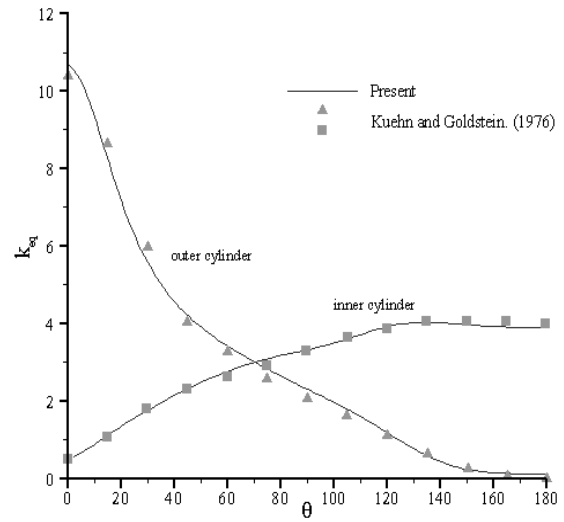### 3.2.2. Natural convection in a concentric annulus with outer circular cylinder

In order to further validate the presented thermal boundary condition, natural convection in a horizontal concentric annulus at different values of the Rayleigh number is tested. A schematic of this problem is sketched in Fig. 3 (b). As can be seen, the configuration consist of two concentric circular cylinder with inner radius of r_i and outer radius of r_o. The outer cylinder

$Ra = 10^3$

$Ra = 6 \times 10^3$

$Ra = 5 \times 10^4$

(a)   (b)   (a)   (b)
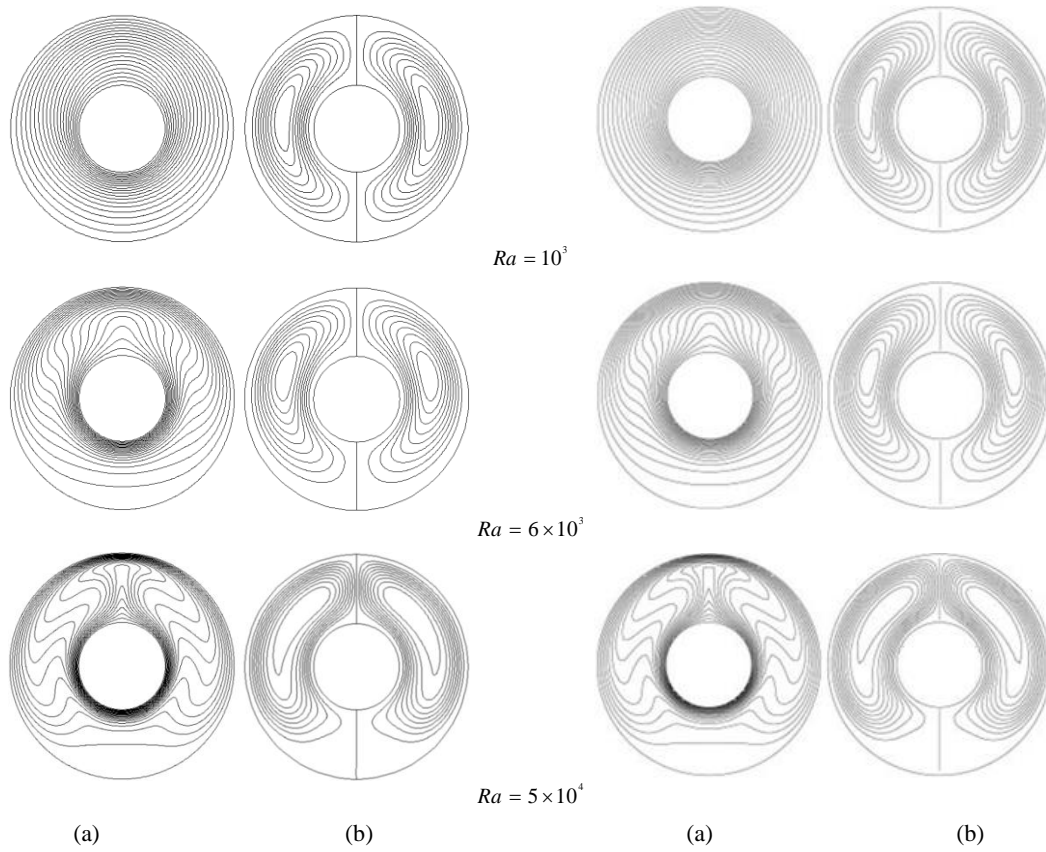
Fig. 6. Comparison of (a) isothermals and (b) streamlines at four different Rayleigh numbers for natural convection phenomenon within an annulus comprised of two concentric circular cylinder, left: present study; right: Duy et al. (2008).
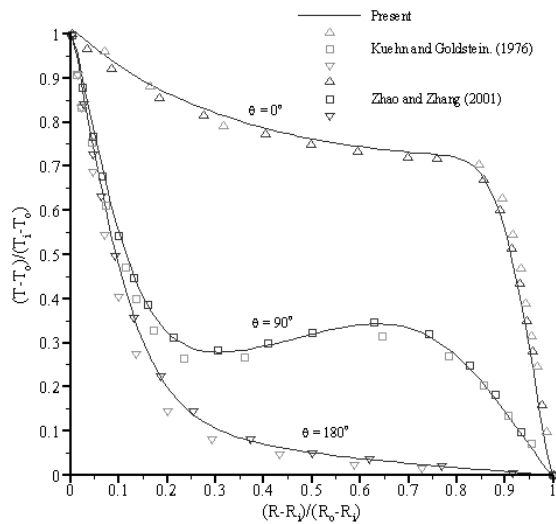
Fig. 7. Comparison of radial temperature distribution for natural convection phenomenon within an annulus comprised of two concentric circular cylinders at

$Ra = 4.7 \times 10^4$, Pr = 0.706

Fig. 8. Comparison of local equivalent heat conductivity for natural convection phenomenon within an annulus comprised of two concentric circular cylinders at $Ra = 4.7 \times 10^4$, Pr = 0.706

Table 4 Comparison of $\bar{k}_{eq}$ for the natural convection in concentric annulus with circular outer cylinder

Ra	$\bar{k}_{eq}$			
	Inner		Outer	
	Present work	Kuehn and Goldstein. (1976)	Present work	Kuehn and Goldstein. (1976)
10^3	1.091	1.081	1.101	1.084
3×10^3	1.399	1.404	1.411	1.402
6×10^3	1.721	1.736	1.740	1.735
10^4	1.994	2.01	1.998	2.005
3×10^4	2.668	2.661	2.671	2.643
5×10^4	3.018	3.024	3.042	2.973
7×10^4	3.289	3.308	3.262	3.226

wall is kept at a constant low temperature of T_C, while the inner cylinder wall has a higher constant temperature, say T_H. The aspect ratio between the outer circular cylinder and the inner one is defined as $\lambda = L/2r_i$ and is set to be $\lambda = 0.8$, where, L is the gap between inner and outer cylinder. Moreover, the Boussinesq approximation is adopted here again, and the Rayleigh number varies in the range of $10^3 \le Ra \le 7\times10^4$. Note that, both of the cylinders do not have any movement. We set $r_i = 30$ for the range $10^3 \le Ra \le 10^4$ and $r_i = 40$ for the range of $10^4 \le Ra \le 10^5$. Also a uniform rectangular grid of sizes $2.5r_o$ is used for all cases. Figure 6 represents the isotherms and streamlines pertained to the case

of $\lambda = 0.8$ and for $Pr = 0.706$ and $Ra = 10^3, 6\times10^3, 5\times10^4$. The results given by Duy et al. (2008) are also included for comparison. All the contours contain 21 contour lines whose levels vary linearly from the minimum to maximum values. A detailed physical interpretation of the flow and heat transfer phenomena related to this case study is discussed by Kuehn and Goldstein. (1976). As can be observed, the contours are in very good agreement with those from Duy et al. (2008). Comparison between our results and the experimental data taken from Kuehn and Goldstein (1976) and also the numerical results taken from Zhao and Zhang (2001) for dimensionless radial temperature distribution are presented in Fig. 7.

One may confirm that in terms of accuracy, the achievements of this study exhibit good agreement with those of other researchers. Here, the local equivalent heat conductivity number k_{eq} can be expressed as:

$$k_{eq} = \frac{Nu}{Nu_{con}} = \ln(r_o/r_i)Nu \tag{54}$$

Substituting Eq. (51) into Eq. (54) gives:

$$k_{eq} = \ln(r_o/r_i)\frac{3T_0L_c\sum_l \delta e_B^l \Delta s_l}{c^2 \alpha \Delta T \delta t} \tag{55}$$

$$\bar{k}_{eq} = \frac{1}{2\pi}\int_0^{2\pi} k_{eq}\, d\theta = \ln(r_o/r_i)\frac{3T_0\sum_l \delta e_B^l \Delta s_l}{2\pi c^2 \alpha \Delta T \delta t} \tag{56}$$

By setting L_c as the radius of cylinder r_i, the averaged equivalent heat conductivity number $\bar{k}_{eq}$ can be evaluated as: Note here that, $\Delta T = (T_w - T_\infty)$. Figure 8 compares our results with those reported in the literature for local equivalent heat conductivity at $Ra = 4.7\times10^4$.

As can be seen from Fig. 8, for inner cylinder, the maximum of local heat flux occurs at the bottom while that minimum value occurs at the top, whereas, for outer cylinder, this trend is reversed. As seen, the achievements of the present study are in good quantitative agreement with their equivalents in Kuehn and Goldstein. (1976). 3

In Table 4, the averaged equivalent heat conductivities at various values of the Rayleigh number are presented to compare with numerical results published by Kuehn and Goldstein. (1976). As expected, the values are in very good agreement with those from Kuehn and Goldstein. (1976). It is also found that the averaged equivalent heat conductivity increases with the Rayleigh number.

4. Conclusion

This paper introduces a thermal immersed boundary lattice Boltzmann method based on the work of Wu and Shu (2009), which takes main advantage of the common IBLBM such as simplicity of algorithm and low computational costs. The method is combination of a direct forcing scheme with a double population thermal lattice Boltzmann method. The research is motivated by the desire to increase the ability of LBM in dealing with complex geometries to simulate flows with heat transfer. In this method, an unknown internal energy source term on the boundary points is considered to properly satisfy the constant temperature boundary condition on the curved wall. The presented approach benefits from features such second-order accuracy and easy computation of the Nusselt number. The verification of the presented method was done

using simulation of natural convection heat transfer problems. Excellent accordance between the presented results and those of other experimental and numerical results is observed. It shows the capability of present method as a robust numerical approach to treat heat transfer phenomena within complex geometries.

REFERENCES

Alexander, F.J., S. Chen and J.D. Sterling (1993). Lattice Boltzmann thermohydrodynamics. Physical Review E, 47(4), 2249-2259.

Bartoloni, A., C. Battista, and S. Cabasino (1993). LBE simulation of Rayleigh–Bénard convection on the APE100 parallel processor. Internatinal Journal of Modern Physics C, 4(5), 993-1006.

Chen, Y., H. Ohashi and M. Akiyama, (1994). Thermal lattice Bhatnagar–Gross–Krook model without nonlinear deviations in macrodynamic equations. Physical Review E, 50(6), 2776-2783.

Chen, S., D. Martínez, and R. Mei (1996). On boundary conditions in lattice Boltzmann methods. Physics of Fluids, 8(9), 2527-2536.

Chen, S. and G.D. Doolen (1998). Lattice Boltzmann method for fluid flow. Annual Review of Fluid Mechanics, 30, 329-364.

Cornubert, R., D. d'Humières, D. Levermore (1991). A Knudsen layer theory for lattice gases, Physica D, 47(1-2), 241-247.

De Vahl Davis, G. (1983). Natural convection of air in a square cavity: a benchmark numerical solution. International Journal for Numerical Methods in Fluids, 3(3), 249-264.

D'Orazio, A., M. Corcione and G.P. Celata (2004). Application to natural convection enclosed flows of a lattice Boltzmann BGK model coupled with a general purpose thermal boundary condition. International Journal Thermal Science, 43(6), 575-586.

Feng, Z. and E. Michaelides (2004). The immersed boundary-lattice Boltzmann method for solving fluid-particles interaction problems. Journal of Computational Physics, 195(2), 602–628.

Feng, Z. and E. Michaelides (2005). Proteus : A direct forcing method in the simulations of particulate flows. Journal of Computational Physics, 202(1), 20–51.

Fu, S.C., R.M.C. So, W.W.F. Leung (2012). Linearized-Boltzmann-type-equation-based finite difference method for thermal incompressible flow. Computers & Fluids 69, 67–80.

Fu, S. C., W. W. F. Leung and R. M. C. So (2013). A lattice Boltzmann and immersed boundary scheme for model blood flow in constricted pipes: part 1 – steady flow. Communications in Computational Physics, 14(1), 126-152.

Fu, S. C., W.W. F. Leung and R. M. C. So (2013). A lattice Boltzmann and immersed boundary scheme for model blood flow in constricted pipes: part 2 – pulsatile flow. Communications in Computational Physics, 14(1), 153-173.

Guo, ZL., CG. Zheng and BC.Shi (2002). Discrete lattice effects on the forcing term in the lattice Boltzmann method, Physical Review E, 65(4), 046308.

He, X., S. Chen, and G.D. Doolen (1998). A novel thermal model for the lattice Boltzmann method in incompressible limit. Journal of Computational Physics, 146(1), 282-300.

Hortmann, M., M. Peric and G. Scheuerer (1990). finite volume multigrid prediction of laminar natural convection: bench-mark solutions. International Journal for Numerical Methods in Fluids, 11, 189–207.

Jeong, H.K., H.S. Yoon, M.Y. Ha and M. Tsutahara (2010). An immersed boundary-thermal lattice Boltzmann method using an equilibrium internal energy density approach for the simulation of flows with heat transfer. Journal of Computational Physics, 229(7), 2526-2543.

Kang, S.K. and Y.A. Hassan (2010). A comparative study of direct-forcing immersed boundary-Lattice Boltzmann methods for stationary complex boundaries. International Journal for Numerical Methods in Fluids, 66(9), 1132-1158.

Kang, S.K. & Y.A. Hassan (2011). A direct-forcing immersed boundary method for the thermal lattice Boltzmann method. Computers & Fluids, 49(1), 36-45.

Kao, P.-H. and R.-J. Yang (2008). An investigation into curved and moving boundary treatments in the lattice Boltzmann method. Journal of Computational Physics, 227(11), 5671-5690.

Khazaeli, R., S. Mortazavi, M. Ashrafizaadeh (2013). Application of a ghost fluid approach for a thermal lattice Boltzmann method. Journal of Computational Physics, 250(Oct.), 126–140.

Kim, B.S., D.S. Lee, M.Y. Ha and H.S. Yoon (2008). A numerical study of natural convection in a square enclosure with a circular cylinder at different vertical locations. International Journal of Heat Mass Transfer, 51(7-8), 1888-1906.

Kuehn, T.H. and R.J. Goldstein (1976). An experimental and theoretical study of natural convection in the annulus between horizontal concentric cylinders, Journal of Fluid Mechanics, 74(4), 695-719.

Li, Q., Y.L. He, Y. Wang and G.H. Tang (2008). An improved thermal lattice Boltzmann model for flows without viscous heat dissipation and

compression work, International Journal of Modern Physics C, 19(01), 125-150.

Liu, C.H., K.H. Lin, H.C. Mai and C.A. Lin (2010). Thermal boundary conditions for thermal lattice Boltzmann simulations, Computers & Mathematics with Applications 59(7), 2178-2193.

Mai-Duy, N., K. Le-Cao and T. Tran-Cong (2008). A Cartesian grid technique based on one-dimensional integrated radial basis function networks for natural convection in concentric annuli, International Journal for Numerical Methods in Fluids, 57(12), 1709-1730.

Margnat, F. and V. Morinière (2009). Behavior of an immersed boundary method in unsteady flows over sharp-edged bodies. Computers & Fluids, 38(6), 1065-1079.

McNamara, G. and B. Alder (1993). Analysis of the lattice Boltzmann treatment of hydrodynamics. Physica A: Statistical Mechanics and its Applications, 194(1-4), 218- 228.

Mittal, R. and G. Iaccarino (2005). Immersed boundary methods, Annual Review of Fluid Mechanics, 37, 239-261.

Moukalled, F. and S. Acharya, (1996). Natural convection in the annulus between concentric horizontal circular and square cylinders. Journal of Thermophysics and Heat Transfer, 10(3), 524-531.

Niu, X.D., C. Shu, Y.T. Chew and Y. Peng (2006). A momentum exchange-based immersed boundary-lattice Boltzmann method for simulating incompressible viscous flows. Physics Letters A, 354(3), 173-182.

Noble, D.R., S. Chen, J.G. Georgiadis and R.O. Buckius (1995). A consistent hydrodynamic boundary condition for the lattice Boltzmann method. Physics of Fluids, 7(1), 203-209.

Peng, Y., C. Shu, and Y.T. Chew, (2003). Simplified thermal lattice Boltzmann model for incompressible thermal flows. Physical Review E, 68(026701), 1-8.

Peng, Y., C.Shu, Y.T. Chew, X.D. Niu and X.Y. Lu (2006). Application of multi-block approach in the immersed boundary-lattice Boltzmann method for viscous fluid flows. Journal of Computational Physics, 218(2), 460-478.

Peskin, C.S. (1972). Flow patterns around heart valves: a numerical method. Journal of Computational Physics, 10(2), 252-271.

Qian, Y.H., D. d. 'Humières and P. Lallemand (1992). Lattice BGK model for Navier-Stokes equation. Europhysics Letters, 17(6), 479.

Rahmati, A. R., M. Ashrafizaadeh and E. Shirani (2014). A multi-relaxation-time lattice Boltzmann method on non-uniform grids for large Eddy simulation of Rayleigh-Bénard convection using two sub-grid scale models. Journal of Applied Fluid Mechanics, 7(1), 89-102.

Shan, X. (1997). Simulation of Rayleigh–Bénard convection using a lattice Boltzmann method, Physical Review E, 55(3), 2780-2787.

Shi, Y., T.S. Zhao and Z.L. Guo (2004). Thermal lattice Bhatnagar-Gross-Krook model for flows with viscous heat dissipation in the incompressible limit. Physical Review E, 70(1), 066310.

Seta Takeshi (2013). Implicit temperature-correction-based immersed-boundary thermal lattice Boltzmann method for the simulation of natural convection, Physical Review E 87, 063304.

Shu, C. and Y.D. Zhu, (2002). Efficient computation of natural convection in a concentric annulus between an outer square cylinder and an inner circular cylinder. International Journal for Numerical Methods in Fluids, 38, 429-445.

Tang, G.H., W.Q. Tao and Y.L. He (2005). Thermal boundary condition for the thermal lattice Boltzmann equation. Physical Review E, 72(01), 016703.

Teixeira C., H., Chen, and DM. Freed (2000). Multi-speed thermal lattice Boltzmann method stabilization via equilibrium under-relaxation, Comput. Phys. Comm., 129(1/3), 207–226.

Wang, JK., M. Wang and ZX. Li (2007). A lattice Boltzmann algorithm for fluid-solid conjugate heat transfer. International Journal of Thermal Science, 46(3), 228-234.

Wu, J. and C. Shu (2009). Implicit velocity correction-based immersed boundary-lattice Boltzmann method and its applications. Journal of Computational Physics, 228(6), 1963-1979.

Yang, X., X. Zhang, Z.Li, GW He(2009). A smoothing technique for discrete delta functions with application to immersed boundary method in moving boundary simulations. Journal of Computational Physics, 228(20), 7821-7836.

Zhao, Y. and B.L. Zhang (2001). A high-order characteristics upwind FV method for incompressible flow and heat transfer simulation on unstructured grids. Computer Methods in Applied Mechanics and Engineering, 190(5-7), 523-536.

Ziegle, D.P. r. (1993). Boundary conditions for lattice Boltzmann simulations. Journal of Statical Physics, 71(5-6), 1171-1177.

Zou, Q. and X. He (1997). On pressure and velocity boundary conditions for the lattice Boltzmann BGK model. Physics of Fluids, 9(6), 1591-15.